JOURNAL OF AGRICULTURAL AND FOOD CHEMISTRY

Matching Avrami Indices Achieves Similar Hardnesses in Palm Oil-Based Fats

ANAND P. SINGH,[†] CONSTANTIN BERTOLI,[§] PHILIPPE R. ROUSSET,[#] AND ALEJANDRO G. MARANGONI*,[†]

Department of Food Science, University of Guelph, Guelph, Ontario N1G 2W1, Canada; Nestlé Product Technology Centre Kemptthal, Nestec Ltd., Kemptthal, Switzerland; and Nestlé Research Center Lausanne, Nestec Ltd., Lausanne, Switzerland

This study demonstrates how chemically interesterified hydrogenated palm oil (IHPO) and partially hydrogenated palm oil (PHPO) can be structured to have similar mechanical properties. Crystallization of IHPO at 30 °C for 24 h yielded a fat with a solid fat content (SFC) of 45% and a yield force of 51.5 N. On the other hand, PHPO had a SFC of 50% and a yield force of 44 N when crystallized under the same conditions. The result was opposite from what would be expected from the SFC point of view, thus suggesting that the microstructure of the fat plays a key role in determining mechanical properties. By matching crystallization behavior using the Avrami index as a guide, microstructures and material hardness were successfully matched. These results suggest that the dynamics of structure formation was a key factor influencing the macroscopic mechanical properties of palm oil-based fats.

KEYWORDS: Crystallization; fat; fractal dimension; yield force; elastic constant; rheology; microstructure; polarized light microscopy

INTRODUCTION

The textural attributes of margarines and spreads are a key factor influencing consumer acceptability. Thus, an understanding of the relationship between crystallization behavior, microstructure, and mechanical properties of fats is required for a successful substitution of one fat with another (*1*).

Even though fats may have similar solid fat contents (SFC) in a particular temperature range, their crystallization behavior, microstructure, and mechanical properties may be vastly different (*2*). Previous investigations have concentrated on different aspects of crystallization kinetics of palm oil (*3*, *4*) and palm oil in sunflower mixtures (*5*), as well as palm oil polymorphism (*6*, *7*). Only one study exists on the relationships between crystallization behavior, microstructure, and mechanical properties in palm oil (*8*).

The objectives of this work were to assess the crystallization behavior, microstructure, and mechanical properties of chemically interesterified hydrogenated palm oil (IHPO), partially hydrogenated palm oil (PHPO), and a partially hydrogenated blend of palm oil and palm stearine [PH(PO/PS)] and an attempt to match material hardness by matching crystallization behavior.

* Corresponding author [e-mail amarango@uoguelph.ca; telephone (519) 824-4120, ext. 54340; fax (519) 824-6631].
[†] University of Guelph.
[§] Nestec Ltd., Kemptthal.
[#] Nestec Ltd., Lausanne.

EXPERIMENTAL PROCEDURES

Source Materials. IHPO, PHPO, and PH(PO/PS) were the three fat samples supplied by Nestlé Product Technology Centre Kemptthal, Nestec Ltd., Kemptthal, Switzerland.

Pulsed Nuclear Magnetic Resonance (pNMR) Spectroscopy. SFC was measured by pNMR using a Bruker PC20 series NMR analyzer (Bruker, Mississauga, Canada). The water bath based cooling used in the pNMR experiments also offered rapid cooling and accurate temperature control.

Two methods were used to obtain the SFC of the given fat: (i) AOCS official method Cd 16-81 (*Official Methods and Recommended Practices of the American Oil Chemists' Society*, 4th ed.; AOCS Press: Champaign, IL, 1993) and (ii) isothermally as a function of time. The AOCS method is dependent upon the tempering history of the sample before measurement, and departures from the procedure will cause variations in results. The fat samples were heated at 130 °C for 10 min before analysis to destroy any crystal history, according to AOCS official method Cc 6-25 (*Official Methods and Recommended Practices of the American Oil Chemists' Society*, 4th ed.; AOCS Press: Champaign, IL, 1993). Three replicates of each melted fat sample in a glass NMR tube (∼2.5 g) were placed in a thermostated water bath at 30, 35, and 40 °C, and SFC readings were obtained at appropriate time intervals.

The crystallization curves obtained under isothermal conditions at 30, 35, and 40 °C were fitted to the Avrami equation by least-squares nonlinear regression (*9*, *10*). The Avrami equation (*11*−*13*) can be used to quantify crystallization kinetics and give an indication of the nature of the crystallization growth process. It has the form

$$\mathrm{SFC}(t)/\mathrm{SFC}(\infty) = 1 - \mathrm{e}^{-kt^n} \quad (1)$$

10.1021/jf034653l CCC: $27.50
Published on Web 02/28/2004

where SFC(t) describes the SFC as a function of time, SFC(∞) is the limiting SFC as time approaches infinity, k is the Avrami constant, and n is the Avrami exponent.

Half-times of crystallization ($t_{1/2}$) were calculated according to the following relationship:

$$t_{1/2} = (0.693/k)^{1/n} \quad (2)$$

Cloud Point Analysis. When fat is cooled isothermally, different fractions of fats are crystallized because of their limited solubility in the remaining liquid fat. A fats and oil analyzer PSA-70V-HT (Phase Technology, Richmond, BC, Canada) was utilized to determine induction times of nucleation (τ), the time at which large increases in the intensity of scattered light were observed. The analyzer required a 150 μL sample per analysis.

The fat sample was melted at 130 °C in an oven and held at this temperature for 10 min, to remove any crystal memory in the sample. One hundred and fifty microliters of the melted fat was pipetted into the preheated sample cup (step 1) of the analyzer. In step 1 of the cloud point analysis, the fat sample in the analyzer was warmed to 69 °C (starting at room temperature) at a rate of 30 °C/min and held at 69 °C for 600 s. In step 2, the sample was cooled (from 69 °C) to 30, 35, or 40 °C at 30 °C/min. The sample was then held at this temperature for 10000 s to monitor crystallization. The induction time of nucleation (τ) was determined by extrapolating from the linearly increasing portion of the curve to the time axis (*14*, *15*). This value is a good and reproducible approximation of the time interval between the moment crystallization temperature is reached and the start of crystallization.

Polarized Light Microscopy (PLM). Fat microstructure was observed by PLM using an Olympus BH polarized light microscope (Olympus, Tokyo, Japan). The microstructures of samples of IHPO, PHPO, and PH(PO/PS) were imaged at 30, 35, or 40 °C. Slides were prepared by melting the fats at 130 °C for 10 min. A preheated Pasteur pipet was used to deposit a small droplet (~10 μL) of fat onto a glass slide preheated to the temperature of the molten fat. A similarly heated glass cover slip was then placed on the surface of the droplet. Samples were then cooled on a Linkam LTS-350 hot/cold stage (Linkam Instruments, Tadworth, U.K.) from 130 to 30, 35, or 40 °C at 30 °C/min and observed under the microscope for up to 100 min. Images were automatically captured every 15 s. Samples were then stored overnight for 24 h, and a final image was taken at that time. A green filter (Hoya Inc., Tokyo, Japan) was placed over the field iris during analysis. PLM images were acquired using a Sony XC-75 CCD video camera (Sony Corp., Tokyo, Japan), an LG-3 PCI frame grabber, and Scion Image software (Scion Corp., Frederick, MD). An automatic blank field subtraction and averaging of 16 frames per image were performed using the computer software. There are a variety of methods used to measure the fractal dimension (D).

In this study two methods, particle counting (*8*, *16*) and box counting (*17*, *18*), were used to determine D. For determination of fractal dimensions by particle counting (D_f), images were inverted and thresholded using Adobe Photoshop (Adobe Systems Inc., San Jose, CA). The threshold level was that which was found to most accurately reflect the original gray scale images. Particle counting was performed for each image using macros written in NIH image as previously described (*8*, *16*). The slope of the log−log plot of the number of particles counted within box sizes of various lengths corresponds to D_f.

The box-counting dimension estimation method (Truesoft International, St. Petersburg, FL, http://www.trusoft.com) was used to determine D_b in terms of a grid-type box-counting method, as previously shown (*17*, *18*). The images were not inverted, but thresholded in Adobe Photoshop prior to analysis.

Large Deformation Mechanical Studies. Rheological properties of the fats under large deformations were determined at 30 °C using an SMS materials tester model MT-LQ (Stable Micro Systems, Surrey, U.K.). The materials tester was calibrated with a 10 kg weight using a 50 kg (500 N) load cell. The liquefied fat was poured into prechilled PVC molds (30, 35, or 40 °C) and crystallized prior to measurement. Disk-shaped samples were prepared, which were 0.6 cm thick and 1 cm in diameter. The parallel plate geometry was positioned at the top of the sample and then lowered at a constant rate of deformation (10 mm/s). The yield force values from the force−deformation profiles were determined using the system software.

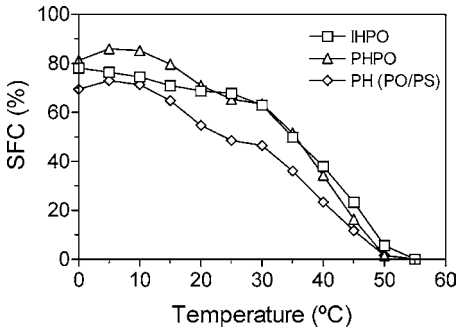

Figure 1. Solid fat content versus temperature profile for IHPO, PHPO, and PH(PO/PS). Symbols represent the average of three replicates and standard deviations of three replicates, typically <1%.

RESULTS AND DISCUSSION

Equilibrium SFC. Figure 1 shows the equilibrium SFCs as a function of temperature for the three fats between 0 and 55 °C. PH(PO/PS) had a lower SFC at each temperature as compared to the other two fat samples. The SFC decreased in a linear fashion as temperature increased from 10 to 25 °C, followed by a small region between 25 and 30 °C with a less accentuated slope. Between 30 and 50 °C, the SFC again decreased linearly with temperature. PHPO had higher SFCs between 0 and 20 °C, whereas IHPO has higher SFCs between 30 and 50 °C. In the case of PHPO and IHPO, melting between 0 and 30 °C was less pronounced than in PH(PO/PS), whereas the SFC decreased linearly with temperature between 30 and 50 °C.

Crystallization Kinetics. Differences in the crystallization kinetics of IHPO, PHPO, and PH(PO/PS) under isothermal conditions were investigated by following increases in SFC with time (**Figure 2**). All three fat samples crystallized very rapidly at 30 °C, whereas increases in SFC in time could not be detected at 40 °C for PHPO and PH(PO/PS). Crystallization kinetics were characterized by fitting the Avrami equation to the crystallization data using nonlinear regression (**Figure 2**). The equation fit the data very well over the entire crystallization range—correlation coefficients were always >0.98. The Avrami constants (k), Avrami exponents (n), and half-times of crystallization ($t_{1/2}$) determined from the curve fits are shown in **Table 1**. As expected, k decreased with increasing crystallization temperature. In IHPO above 35 °C, crystallization temperature had a very strong influence on k—the Avrami constant dropped by a factor of roughly 10^4. In PHPO and PH(PO/PS) above 30 °C crystallization temperature also had a very strong influence on k—the Avrami constant dropped by factors of roughly 10^4 in PHPO and 10^6 in PH(PO/PS). The increase in $t_{1/2}$ for the three fats as a function of increasing crystallization temperature reflects the decrease in k at higher temperatures (**Table 1**).

The sharp change in Avrami exponent around 40 °C in IHPO and 35 °C in PHPO and PH(PO/PS) suggests the existence of different crystallization mechanisms depending on the degree of supercooling. The change in n at this point could indicate differences in crystal growth geometry and possibly the type of nucleation. An increase in the induction time and a more sigmoidal crystallization curve is generally indicated by a higher Avrami index (*8*, *10*, *18*). This was found to be true—at higher temperatures, values of $t_{1/2}$ and n were significantly higher and crystallization curves appeared to be more sigmoidal. Generally,

Table 1. Avrami Constants (k), Avrami Exponents (n), and Half-Times of Crystallization ($t_{1/2}$) for IHPO, PHPO, and PH(PO/PS) at 30, 35, and 40 °C[a]

	IHPO			PHPO			PH(PO/PS)		
temp (°C)	k (t^{-n})	n	$t_{1/2}$ (min)	k (t^{-n})	n	$t_{1/2}$ (min)	k (t^{-n})	n	$t_{1/2}$ (min)
30	0.57 SD = 0.044 n = 3	0.60 SD = 0.024 n = 3	1.39 SD = 0.162 n = 3	0.29 SD = 0.043 n = 3	0.87 SD = 0.056 n = 3	2.78 SD = 0.30 n = 3	0.13 SD = 0.028 n = 3	1.24 SD = 0.091 n = 3	3.92 SD = 0.302 n = 3
35	0.16 SD = 0.027 n = 3	0.97 SD = 0.055 n = 3	4.44 SD = 0.378 n = 3	1.35E–05 SD = 1.002E–05 n = 3	3.22 SD = 0.194 n = 3	29.16 SD = 1.014 n = 3	4.83E–07 SD = 1.72E–7 n = 3	4.15 SD = 0.098 n = 3	30.57 SD = 0.308 n = 3
40	6.09E–05 SD = 8.45E–05 n = 3	2.71 SD = 0.479 n = 3	31.56 SD = 1.817 n = 3						

[a] Indicated are the average and standard deviation (SD) of n replicates.

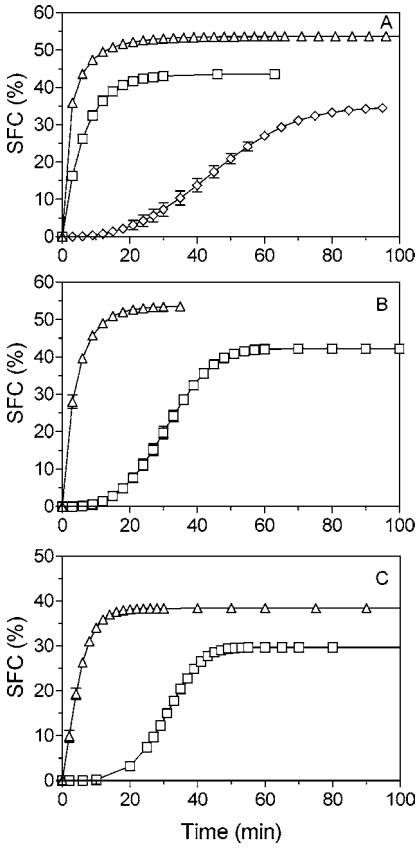

Figure 2. Solid fat content versus time profile during isothermal crystallization of IHPO (**A**), PHPO (**B**), and PH(PO/PS) (**C**) at 30 °C (△), 35 °C (□), and 40 °C (◇). Symbols represent the average of three replicates and their standard deviation.

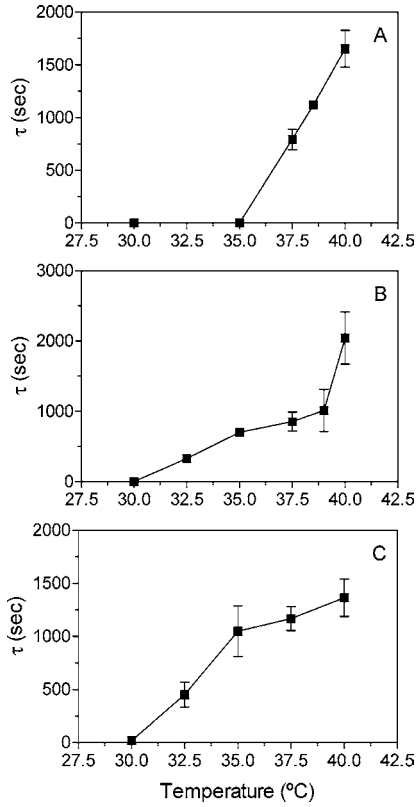

Figure 3. Induction time of nucleation (τ) versus crystallization temperature for IHPO (**A**), PHPO (**B**), and PH(PO/PS) (**C**). Values represent the average and standard deviation of three replicates.

as the rate of crystallization increases, the growth mechanism changes from a one- to a multidimensional event, as reflected by an increase in the Avrami exponent. An increase in the Avrami exponent can also be due to a change in the type of nucleation, from more instantaneous at higher degrees of supercooling to more sporadic at lower degrees of supercooling (*8*, *10*).

The maximal SFC value at each isothermal crystallization temperature was not comparable to that arrived at in the equilibrium melting profile of **Figure 1**. Therefore, the manner in which the fat is crystallized is very important. In the AOCS method the fat sample is tempered prior to measurements being taken, whereas in isothermal crystallization experiments, molten samples are plunged directly to the desired temperature without tempering.

The similarities in the Avrami exponents of IHPO crystallized at 35 and 40 °C and those of PHPO crystallized at 30 and 35 °C, respectively, suggest similar growth modes at these different temperatures. The distinct change in Avrami exponent for IHPO at ∼40 °C and for PHPO and PH(PO/PS) at ∼35 °C suggests a change in the crystal growth, and/or nucleation, mechanism in these fats.

Crystallization kinetics were also examined using a cloud point analyzer. Temperature had a significant effect on the induction time of nucleation (τ). The nucleation rate decreased rapidly with increasing temperature. The temperature-dependent supersaturation is the driving force of nucleation. In IHPO, the induction time between 30 and 35 °C was too short to be determined; that is, the nucleation process was very rapid in this temperature range (**Figure 3A**). The induction time

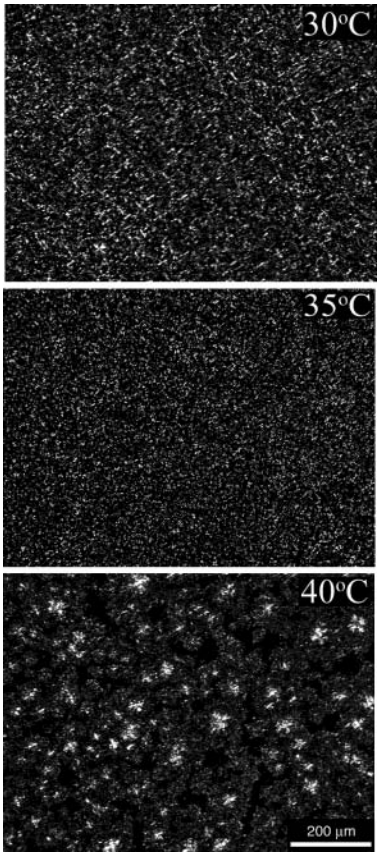

Figure 4. Polarized light micrographs of IHPO crystallized isothermally at 30 °C (**A**), 35 °C (**B**), and 40 °C (**C**) for 24 h. Bar represents 200 μm.

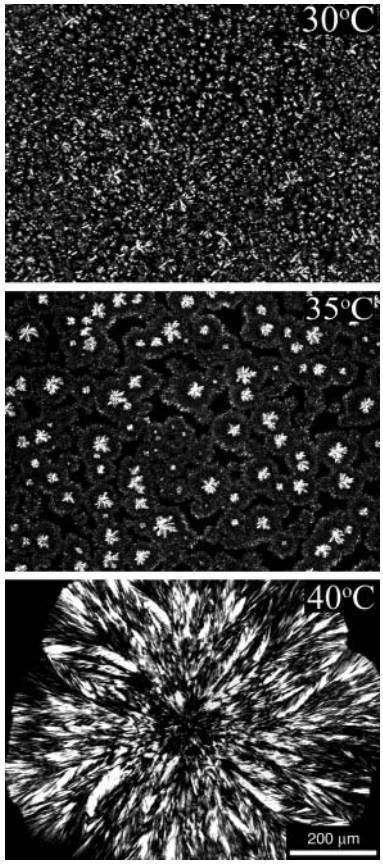

Figure 5. Polarized light micrographs of PHPO crystallized isothermally at 30 °C (**A**), 35 °C (**B**), and 40 °C (**C**) for 24 h. Bar represents 200 μm.

increased sharply with increases in temperature between 35 and 40 °C. In PHPO there was a gradual increase in induction time with increase in temperature from 30 to 39 °C. A sharp rise in induction time was noticed beyond 39 °C (**Figure 3B**). In the case of PH(PO/PS), a sharp increase in induction time was noticed between 30 and 35 °C and a gradual increase beyond 35 °C (**Figure 3C**). The plot of τ versus temperature for the three samples yielded two distinct linear regions with discontinuities occurring at 35 °C (IHPO), 39 °C (PHPO), and 35 °C [PO(PH/PS)]. Ng (*4*) observed instantaneous nucleation in a palm oil melt at 15 °C and an abrupt discontinuity in a time−temperature curve at 24 °C indicative of the nucleation of a different polymorphic form. Putte et al. (*3*) have reported the primary nucleation rate of the β'-polymorphic form is high compared to that of the β-polymorphic form below 35 °C in palm oil.

Microstructure and Quantification of Microstructure Using Fractal Analysis. The microstructures of the three fats crystallized isothermally at 30, 35, and 40 °C were imaged using polarized light microscopy. The change in microstructure with increasing temperature (decrease in the degree of supercooling) can be due to changes in the nucleation rate, the formation of crystals in a different polymorphic form, due to fractionation, or some combination of the above. A decreased nucleation is usually accompanied by an increase in crystal growth (*19*). In IHPO (**Figure 4**), a rapid and extensive nucleation was evident at 30 and 35 °C. At 40 °C, the initial number of nuclei present is lower, and crystal growth begins to make a more significant contribution to crystallization. **Figure 5** shows that a combination of small spherulites and small needles was present in the PHPO sample at 30 °C. Moreover, the micrograph at 35 °C resembles the micrograph of IHPO at 40 °C. By 40 °C, large spherulitic microstructures of ~200 μm in diameter were present in PHPO. Similarly, for the isothermal crystallization of PH(PO/PS) (**Figure 6**), a combination of small spherulites and small needle-shaped crystals was observed at 30 °C. At 35 °C, large empty spaces with a cloudlike formation of fine granular crystallites were observed. Large spherulitic microstructures were visible at 40 °C, similar to those observed in PHPO at 40 °C. Spherulite formation is favored by low nucleation density, high medium viscosity, and the presence of dissolved impurities (*20*). Kawamura (*6*) has reported the nucleation of daughter crystals on the surface of parent spherulites under isothermal conditions and observed similar crystal morphologies below 24 °C (granular) and above 26 °C (dendritic spherulites). Values for the Avrami exponent increased dramatically as a function of temperature for all three fats (**Table 1**). The increase in Avrami exponent indicates a change in crystallization mode (nucleation type and dimensionality of growth). These results are in general agreement with other similar studies on different fat systems (*21*, *22*).

The concept of fractals (*23*−*25*) was used to quantify microstructure by microscopy and image analysis using particle counting and box-counting procedures. **Table 2** shows the values of D_f and D_b for isothermal crystallization at 30, 35, and 40 °C. In general, an increase in temperature led to a decrease in both D_f and D_b. Thus, it was possible to quantify differences in general microstructure using fractal image analysis. Analysis was not carried out on micrographs, which depicted a single spherulite or large crystallite, because we are interested in the spatial distribution of mass within the network. A single large crystal does not constitute a network. This was the case for PHPO samples crystallized at 40 °C.

Table 2. Fractal Dimensions Determined by Particle Counting (D_f) and Box Counting (D_b) for IHPO, PHPO, and PH(PO/PS) Crystallized Isothermally at 30, 35, and 40 °C

	D_f			D_b		
	30 °C	35 °C	40 °C	30 °C	35 °C	40 °C
IHPO	2.0 SD = 0.0026 $n = 5$	1.96 SD = 0.046 $n = 6$	1.94 SD = 0.018 $n = 5$	1.87 SD = 0 $n = 5$	1.87 SD = 0.0013 $n = 6$	1.84 SD = 0.0015 $n = 5$
PHPO	2.01 SD = 0.022 $n = 3$	1.80 SD = 0.061 $n = 5$	nd[a]	1.87 SD = 0.0015 $n = 3$	1.80 SD = 0.018 $n = 5$	nd[a]
PH(PO/PS)	1.94 SD = 0.027 $n = 5$	1.88 SD = 0.016 $n = 5$	1.55 SD = 0.015 $n = 2$	1.86 SD = 0.00083 $n = 5$	1.81 SD = 0.0019 $n = 5$	1.69 SD = 0.018 $n = 2$

[a] Not determined.

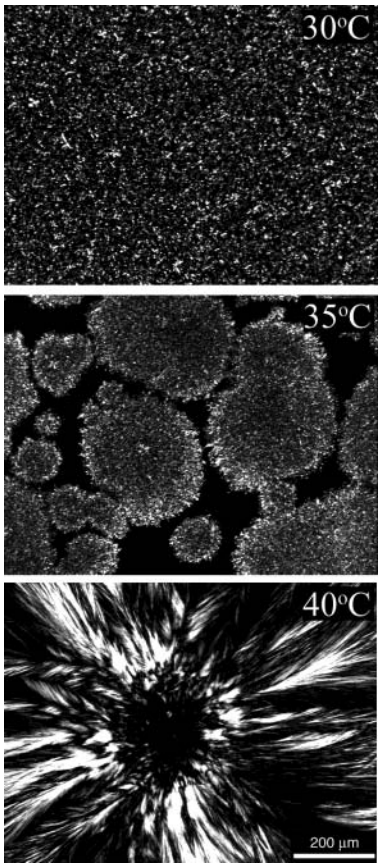

Figure 6. Polarized light micrographs of PH(PO/PS) crystallized isothermally at 30 °C (**A**), 35 °C (**B**), and 40 °C (**C**) for 24 h. Bar represents 200 μm.

Relationship among Crystallization, Microstructure, and Mechanical Properties. In an attempt to establish a relationship among crystallization behavior, microstructure, and mechanical properties, Avrami indices at different temperatures were used as a guide to match the hardness of IHPO and PHPO. Because the Avrami exponent provides an indication of the crystal growth mode, it might correlate with microstructure and, ultimately, mechanical properties. Thus, on the basis of the values of the Avrami index, a specific crystallization scheme was designed geared toward matching the crystallization behaviors of IHPO and PHPO and, we hoped, their mechanical properties (**Figure 7**).

The similarities in *n* for IHPO crystallized at 35 and 40 °C to PHPO crystallized at 30 and 35 °C, respectively, suggested that these fats can crystallize in a similar fashion. Much to our surprise, IHPO that had been crystallized overnight at 35 °C and transferred thereafter to 30 °C and PHPO that had been crystallized overnight at 30 °C (**Figure 7A**, Scheme 1) had similar hardnesses (**Table 3**). IHPO was crystallized overnight at 35 °C and held at 30 °C for 60 min prior to the analysis. The hardnesses of these two fats crystallized under these different conditions were very similar, even though their SFCs were different. Therefore, SFC is not the sole parameter that influences the ultimate strength of fat crystal network. Similarly, we were able to match the hardness of IHPO crystallized at 40 °C and PHPO crystallized at 35 °C (**Figure 7B**, Scheme 2). Both samples were held at 30 °C for 60 min prior to the analysis. Even though in our experiments we used an overnight crystallization period, 60−90 min is deemed to be sufficient for the setting of their fat crystal networks (based on the SFC−time growth curves). Hence, our results suggest that it is possible to substitute one type of fat with another given a slight modification in the cooling method during crystallization.

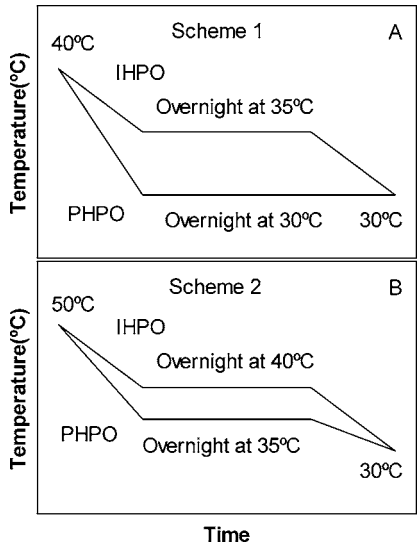

Figure 7. Schematic diagram of crystallization temperature versus time showing how to match the crystallization behaviors of IHPO and PHPO by two different temperature modifications.

Micrographs of the fat samples were also obtained after crystallization of samples as described in Schemes 1 and 2 in **Figure 7** (**Figures 8** and **9**). Fractal analysis was also carried out on the micrographs shown. No significant differences were observed in D_f and D_b ($P > 0.05$) between PHPO and IHPO crystallized as shown in **Figure 7** (**Table 3**). This indicated that by matching the crystallization behaviors of the two fats, we

Table 3. Indicators of Mechanical Strength under Large Deformation for Fat Samples Crystallized As Described in Schemes 1 and 2 of **Figure 7**[a]

IHPO						PHPO					
cryst temp (°C)	yield force (N)	*K* (N/mm)	SFC (%)	D_f	D_b	cryst temp (°C)	yield force (N)	*K* (N/mm)	SFC (%)	D_f	D_b
35/30	42.1 SD = 2.79 *n* = 8	100.8 SD = 27.9 *n* = 6	43.8 SD = 0.24 *n* = 2	1.99 SD = 0.079 *n* = 27	1.86 SD = 0.007 *n* = 27	30	43.6 SD = 3.43 *n* = 7	76.7 SD = 10.83 *n* = 7	53.5 SD = 0.26 *n* = 2	1.99 SD = 0.059 *n* = 9	1.87 SD = 0.0053 *n* = 9
40/30	23.9 SD = 2.66 *n* = 10	45.0 SD = 8.85 *n* = 10	34.9 SD = 0.64 *n* = 2	1.94 SD = 0.096 *n* = 27	1.81 SD = 0.023 *n* = 27	35/30	24.2 SD = 1.93 *n* = 10	43.2 SD = 6.41 *n* = 10	43.7 SD = 1.14 *n* = 2	1.92 SD = 0.104 *n* = 25	1.78 SD = 0.047 *n* = 26

[a] *K*, elastic constant; SFC, solid fat content; D_f, particle counting mass fractal dimension; D_b, box counting mass fractal dimension. Reported are the average and standard deviation (SD) of *n* replicates.

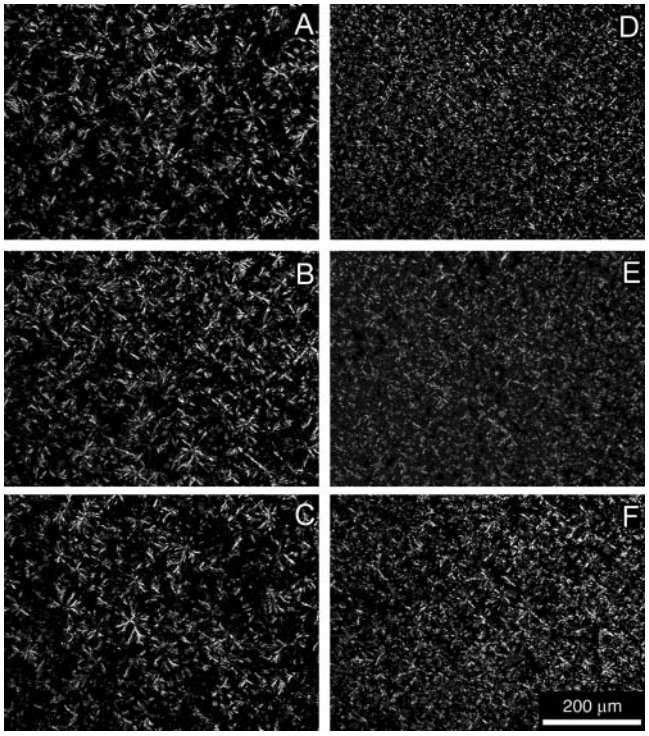

Figure 8. Polarized light micrographs of IHPO and PHPO crystallized at 35 and 30 °C; (**A**, **D**) after immediate crystallization at 35 and 30 °C; (**B**, **E**) 30 °C for 60 min; (**C**, **F**) final imaging done after holding at 30 °C for 24 h.

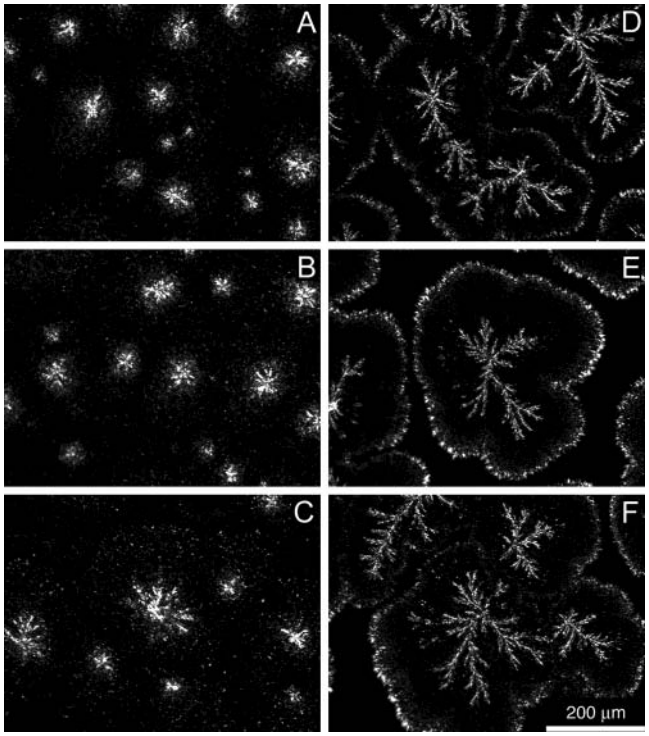

Figure 9. Polarized light micrographs of IHPO and PHPO crystallized at 40 and 35 °C: (**A**, **D**) after immediate crystallization at 40 and 35 °C; (**B**, **E**) 30 °C for 60 min; (**C**, **F**) final imaging done after holding at 30 °C for 24 h.

were able to obtain similar values for the fractal dimensions. This effect could be explained by a "network decoration" hypothesis: after the initial microstructure is created, further growth would then have taken place on top of the existing scaffolding created in the initial stages of nucleation and growth (i.e., decorating the network). This, however, remains to be proven. Crystallization temperature had a significant effect on network structure ($P = 0.0001$) within each fat type. Higher crystallization temperatures led to significant decreases in D_f and D_b in both fat systems ($P = 0.001$), as shown in **Table 3**.

Conclusions. In this study we show that the microstructure of the fat plays a key role in determining mechanical properties. The Avrami index was used as a guide to match the crystallization behaviors of IHPO and PHPO. By matching Avrami indices during the crystallization process, similar hardnesses and spatial distributions of mass in two palm oil-based fats (IHPO and PHPO) were achieved. Thus, it is possible to engineer the mechanical properties of a fat by matching the crystallization growth mode (nucleation and geometry).

LITERATURE CITED

(1) Heertje, I. Microstructural studies in fat research. *Food Struct.* **1993**, *12*, 77−94.

(2) Campos, R.; Narine, S. S.; Marangoni, A. G. Effect of cooling rate on the structure and mechanical properties of milk fat and lard. *Food Res. Int.* **2002**, *35*, 971−981.

(3) van Putte, K. P. A. M.; Bakker, B. H. Crystallization kinetics of palm oil. *J. Am. Oil Chem. Soc.* **1987**, *64*, 1138−1143.

(4) Ng, W. L. A study of the kinetics of nucleation in a palm oil melt. *J. Am. Oil Chem. Soc.* **1990**, *67*, 879−882.

(5) Kloek, W.; Walstra, P.; van Vliet, T. Crystallization kinetics of fully hydrogenated palm oil in sunflower oil mixtures. *J. Am. Oil Chem. Soc.* **2000**, *64*, 389−398.

(6) Kawamura, K. The DSC thermal analysis of crystallization behavior in palm oil. *J. Am. Oil Chem. Soc.* **1979**, *56*, 753−758.

(7) Kawamura, K. The DSC thermal analysis of crystallization behavior in palm oil, II. *J. Am. Oil Chem. Soc.* **1980**, *57*, 48−52.

(8) Litwinenko, J. W.; Rojas, A. M.; Gerschenson, L. N.; Marangoni, A. G. Relationship between crystallization behavior, microstructure, and mechanical properties in a palm oil-based shortening. *J. Am. Oil Chem. Soc.* **2002**, *79*, 647−654.
(9) Marangoni, A. G. On the use and misuse of the Avrami equation in the characterization of fat crystallization process. *J. Am. Oil Chem. Soc.* **1998**, *75*, 1465−1467.
(10) Wright, A. J.; Hartel, R. W.; Narine, S. S.; Marangoni, A. G. The effect of minor components on milk fat crystallization. *J. Am. Oil Chem. Soc.* **2000**, *77*, 463−475.
(11) Avrami, M. Kinetics of Phase Change I. General Theory. *J. Chem. Phys.* **1939**, *7*, 1103−1112.
(12) Avrami, M. Kinetics of Phase Change II. Transformation-Time Relations for Random Distribution of Nuclei. *J. Chem. Phys.* **1940**, *8*, 212−224.
(13) Avrami, M. Kinetics of Phase Change III. Granulation, Phase Change, and Microstructure. *J. Chem. Phys.* **1941**, *9*, 177−184.
(14) Wright, A. J.; Narine, S. S.; Marangoni, A. G. Comparison of experimental techniques used in the study of the crystallization of lipids. *J. Am. Oil Chem. Soc.* **2000**, *77*, 1239−1242.
(15) Wright, A. J.; Narine, S. S.; Marangoni, A. G. Comparison of experimental techniques used in the study of the crystallization of lipids. In *Crystallization and Solidification Properties of Lipids*; Widlak, N., Hartel, R. W., Narine, S. S., Eds.; AOCS Press: Champaign, IL, 2000; pp 120−131.
(16) Wright, A. J.; Marangoni, A. G. The effects of minor components on the structure and mechanical properties of milkfat. *J. Food Sci.* **2003**, *68*, 182−186.
(17) Marangoni, A. G.; Narine, S. S. Identifying key structural indicators of mechanical strength in fractal networks of fat crystals. *Food Res. Int.* **2000**, *35*, 957−969.
(18) Marangoni, A. G.; McGauley, S. The relationship between crystallization behavior and structure in cocoa butter. *Cryst. Growth Design* **2003**, *3*, 95−108.
(19) Herrera, M. L.; Hartel, R. W. Effect of processing conditions on crystallization kinetics of a milk fat model system. *J. Am. Oil Chem. Soc.* **2000**, *77*, 1177−1187.
(20) Sharples, A. Overall Kinetics of Crystallization. *Introduction to Polymer Crystallization*; Edward Arnold: London, U.K., 1966; pp 44−59.
(21) Herrera, M. L.; Galabella, C.; Melgarejo, M.; Anon, M. C. Isothermal crystallization of hydrogenated sunflower oil: II. Growth and solid fat content. *J. Am. Oil Chem. Soc.* **1999**, *76*, 1−6.
(22) Martini, S.; Herrera, M. L.; Hartel, R. W. Effect of cooling rate on crystallization behavior of milk fat fraction/sunflower oil blends. *J. Am. Oil Chem. Soc.* **2002**, *79*, 1055−1062.
(23) Narine, S. S.; Marangoni, A. G. Fractal nature of fat crystal networks. *Phys. Rev. E* **1999**, *59*, 1908−1920.
(24) Marangoni, A. G.; Rousseau, D. Is plastic fat rheology governed by the fractal nature of the fat crystal network? *J. Am. Oil Chem. Soc.* **1996**, *73*, 991−994.
(25) Marangoni, A. G. The nature of fractality in fat crystal networks. *Trends Food Sci. Technol.* **2002**, *13*, 37−47.

Received for review June 19, 2003. Revised manuscript received December 10, 2003. Accepted January 26, 2004.

JF034653L